2012

Insight into the Modulation of Shaw2 Kv Channels by General Anesthetics: Structural and Functional Studies of S4-S5 linker and S6 C-terminal peptides in micelles by NMR

Jin Zhang
Georgia State University, jzhang22@gsu.edu

Xiaoguang Qu
Iowa State University

Manuel Covarrubias
Thomas Jefferson University, Manuel.Covarrubias@jefferson.edu

Markus W. Germann
Georgia State University, mwg@gsu.edu

Recommended Citation

Insight into the modulation of Shaw2 Kv channels by general anesthetics: Structural and functional studies of S4–S5 linker and S6 C-terminal peptides in micelles by NMR

Jin Zhang [a,1], Xiaoguang Qu [b,1], Manuel Covarrubias [c,e], Markus W. Germann [a,d,*]

[a] Department of Chemistry, Georgia State University, Atlanta, GA 30303, USA
[b] Department of Genetics, Development, and Cell Biology, Iowa State University, Ames, IA 50011, USA
[c] Department of Neuroscience, Jefferson Medical College of Thomas Jefferson University, Philadelphia, PA 19107, USA
[d] Department of Biology, Georgia State University, Atlanta, GA 30303, USA
[e] Farber Institute for Neuroscience, Jefferson Medical College of Thomas Jefferson University, Philadelphia, PA 19107, USA

ARTICLE INFO

ABSTRACT

The modulation of the *Drosophila* Shaw2 Kv channel by 1-alkanols and inhaled anesthetics is correlated with the involvement of the S4–S5 linker and C-terminus of S6, and consistent with stabilization of the channel's closed state. Structural analysis of peptides from S4–S5 (L45) and S6 (S6c), by nuclear magnetic resonance and circular dichroism spectroscopy supports that an α-helical conformation was adopted by L45, while S6c was only in an unstable/dynamic partially folded α-helix in dodecylphosphocholine micelles. Solvent accessibility and paramagnetic probing of L45 revealed that L45 lies parallel to the surface of micelles with charged and polar residues pointing towards the solution while hydrophobic residues are buried inside the micelles. Chemical shift perturbation introduced by 1-butanol on residues Gln320, Thr321, Phe322 and Arg323 of L45, as well as Thr423 and Gln424 of S6c indicates possible anesthetic binding sites on these two important components in the channel activation apparatus. Diffusion measurements confirmed the association of L45, S6c and 1-butanol with micelles which suggests the capability of 1-butanol to influence a possible interaction of L45 and S6c in the micelle environment.

© 2012 Elsevier B.V. All rights reserved.

1. Introduction

Voltage-gated potassium (Kv) channels comprise a large family of potassium channels, which are vitally important in the regulation of electrical signaling in a variety of excitable cells [1]. Utilizing the combination of genomic and biophysical techniques, a growing number of discoveries have linked Kv channel mutations with a number of diseases [1–4].

Kv channels share a similar structural topology. They are tetramers formed from four identical subunits each having six transmembrane-helices (S1–S6). The first four helices (S1–S4) form a voltage sensing domain (VSD), that detects voltage difference across cell membranes via charged amino acids. The S5 and S6 segments of all four subunits form a pore domain where the S5–S6 linkers (P-loop) act as an extracellular selectivity filter while the S6 C-termini of all subunits make up the intracellular pore portal [5]. Numerous studies suggest that opening and closing of the Kv channel are carried out by coupling the conformational changes of the VSD and S6 C-termini through the S4–S5 linker [6–16]. This necessitates conformational malleability and correct positioning of the S4–S5 linker in order to transmit the coupling between the VSD and S6 C-terminus.

Their involvement in vital biological processes and disease states render Kv channels important targets for drug therapy [3,17]. Numerous small molecules and drugs have been found to interact with Kv channels. On the extracellular side, the P-loop and adjacent residues of S5 and S6 are binding sites for toxins and channel blockers [18,19]. Binding sites for small molecules are also located on the intracellular side of S5 and S6 [20,21].

The *Drosophila* Shaw2 is a neuronal Kv channel that is closely related to the mammalian Kv3 channels [22]. The Shaw2 channel is selectively inhibited by 1-alkanols and halothane at pharmacologically relevant concentrations [23–25]. The action of the inhibitors is consistent with binding to an intracellular site and the stabilization of the channel's close state [26]. However, the precise molecular interactions governing 1-alkanol binding and the mechanism of channel inhibition are not understood.

The energetics and kinetics of this inhibition have been investigated by applying a combination of biochemical, electrophysiological and

structural methods [27,28]. We have demonstrated that S4–S5 linker of Shaw2 is required for 1-alkanol inhibition. Transplanting just a thirteen amino acid segment from Shaw2 S4–S5 linker into Kv3.4 causes this modified human channel now also to become 1-alkanol responsive [24]. The Shaw2 S4–S5 linker peptide (L45) readily adopts an α-helical structure in solution and in the membrane environment (phospholipid micelles), while the corresponding Kv3.4 peptide does not [27,28]. This links the 1-alkanol response to the α-helical propensity of L45. Additional elements involved in 1-alkanol binding were identified by alanine scanning to be S5 and S6 [29], as demonstrated by the observation that mutating the second Pro in the PVP motif of S6 resulted in suppression of the 1-alkanol inhibition. This was attributed to the destabilization of the closed state [29]. Furthermore, a recent study supports the presence of putative 1-alkanol and halothane binding pockets in interfaces involving the S4–S5 linker, S5 and S6 [30].

Despite numerous functional studies, the precise molecular events governing 1-alkanol modulation are not fully understood due to the lack of direct structural information. Encouraged by previous NMR studies on small linker peptides from Shaker and HERG channels in a micelle environment [31,32], we investigated the participation of the S4–S5 linker and S6 C-terminus in the 1-alkanol modulation of Shaw2 channels by focusing on the following objectives: first, determine the structures of peptides derived from the S4–S5 linker (L45) and S6 C-terminus (S6c) in a membrane-like environment (DPC micelles); second, determine the orientation of the L45 in DPC micelles to understand residue accessibility; and finally, explore potential binding sites of 1-alkanols in micelle bound peptides.

2. Materials

The Shaw2 S4–S5 linker peptide (L45, GLKILIQTFRASA) and S6 C-terminus peptides (S6c, VIVSNFAMYYSHTQ) derived from the voltage-gated *Shaw* potassium channels were purchased from Biopeptide Co., Inc. (San Diego, CA). Deuterated dodecylphosphocholine, DPC-d_{38} (D, 98%) was purchased from CDN Isotopes Inc. (Quebec, Canada). Gadolinium-diethylenetriaminepentaacetic acid bismethylamide (Gd-DTPA-BMA) was from GE Healthcare (Princeton, NJ) as Omniscan™ gadodiamide injection (287 mg/ml). 2,2,2-Trifluoroethanol (TFE, 99.5%) was from Aldrich. TFE-d3 (D, 99.5%) and D_2O (D, 99.9%) were from Cambridge Isotope Laboratories (Andover, MA). 1-Butanol (99%) was from Fisher Scientific (Fair Lawn, NJ). 1,2-Dimyristoyl-*sn*-glycero-3-phosphocholine (DMPC, 99%) and 1,2-dihexanoyl-*sn*-glycero-3-phosphocholine (DHPC, 99%) were from Avanti Polar Lipid, Inc. (Alabaster, AL). Tetradecyltrimethylammonium bromide (TTAB, 99.5%) was from Sigma-Aldrich Co. (St. Louis, MO).

3. Methods

3.1. CD spectroscopy

CD samples were prepared by dissolving peptides in 5 mM sodium phosphate buffer, pH 6.0, to a final concentration of 50 μM unless described otherwise. A JA-810 spectropolarimeter (Jasco, Tokyo, Japan) was used to record all CD spectra at room temperature. Each spectrum was the average of four scans. The resulting spectra were deconvoluted using CDPro [33,34].

3.2. NMR spectroscopy

The micellar NMR samples were prepared by co-dissolving peptides, typically 1 mM with 30 mM DPC-d_{38} in 10 mM sodium phosphate buffer (pH 5.8, unless described otherwise) containing 10% D_2O. For D_2O experiments the samples were lyophilized and resuspended in 100% D_2O. For the paramagnetic sample preparation, Gd-DTPA-BMA

(287 mg/ml) was added to the micellar samples to a final concentration of 2 mM.

All NMR spectra were collected on 500 and 600 MHz Bruker Avance systems using a 5 mm triple resonance (TXI) Z-gradient probe head or TXI cryoprobe (Bruker). For assignments and structure determination, 1D spectra were recorded using presaturation or jump-and-return pulse sequences to suppress solvent (water) signal [35]. 2D NMR experiments: TOCSY, NOESY, and natural abundance ¹H-¹³C-HSQC were recorded with presaturation as appropriate and using time proportional phase increment (TPPI) for quadrature detection in F1. The mixing times were set to 44 ms for TOCSY (2K×512, 32 scans) and 75 and 400 ms for NOESY experiments (2K×512, 32 scans), respectively. NMR spectra were assigned using Sparky [36] following standard methods [37].

To assess the residue accessibilities and the peptide orientation utilizing proton relaxation properties, saturation-recovery NOESY (2K×512, 32 scans) and inversion-recovery ¹H-¹³C-HSQC (2K×128, 32 scans) spectra in the absence and presence of the paramagnetic reagent were recorded. For the saturation recovery NOESY a pulse train was implemented to saturate all protons and cross peak volumes were used to calculate the paramagnetic attenuation A_i of H_α protons. Briefly, NMR cross peak volumes $V_i^{p,d}$ were measured and autoscaled according to the relation [38,39]:

$$v_i^{p,d} = V_i^{p,d} / \left(\sum V_i^{p,d} / n \right) \tag{1}$$

where $v_i^{p,d}$ is the autoscaled peak volume from the sample with (^{p}) and without (^{d}) paramagnetic reagent. $V_i^{p,d}$ is the cross peak volume of the sample with and without paramagnetic reagent; n is the number of cross peaks measured. Paramagnetic attenuations A_i were then calculated according to:

$$A_i = 2 - \frac{v_i^p}{v_i^d}. \tag{2}$$

In the inversion-recovery HSQC, a 180° ¹H pulse followed by a variable recovery delay (τ) precedes a normal HSQC experiment. ¹H T_1 values were obtained via fitting the inversion-recovery HSQC peak intensities to:

$$I = I_0 \left(1 - 2e^{-\tau/T_1} \right) \tag{3}$$

where I is the signal intensity after time τ and I_0 is the fully relaxed signal. The paramagnetic relaxation enhancement (PRE) was then calculated for each residue as the slope of the relaxation rate constant R_1 ($R_1 = 1/T_1$) *vs.* Gd(III)DTPA-BMA concentration plot. The orientation of the peptide helix in the micelle is then obtained by fitting the measured PRE to the equation [40]:

$$PRE = \frac{k\pi}{6\left[A + 1.5 \text{ Å} \cdot \sin(\tau) \cdot (x-1) - 3.25 \cos(\tau) \cdot \cos(1.745(x-1) + \rho)\right]^3} \tag{4}$$

where k is a constant; A is the immersion depth (Å) of the helical axis at the position of the first residue used for calculation in micelles; τ is the angle (rad) between the axis of the peptide helix and the membrane surface; ρ is the angle (rad) between the H_α of the first residue whose PRE data was used to fit Eq. (4) and a line, which is perpendicular to the helix axis and points towards the membrane surface; x is the residue number; 1.5 is the helix pitch per residue; 3.25 is the average radius of the helix measured from H_α; and 1.745 ($2\pi/3.6$) defines the periodicity of 3.6 residues per turn.

Diffusion measurements were carried out using Diffusion-Ordered Spectroscopy (DOSY) [41]. A 1D setup (stegp1s1d) was run prior to DOSY experiments (stegp1s) to optimize parameters: diffusion time
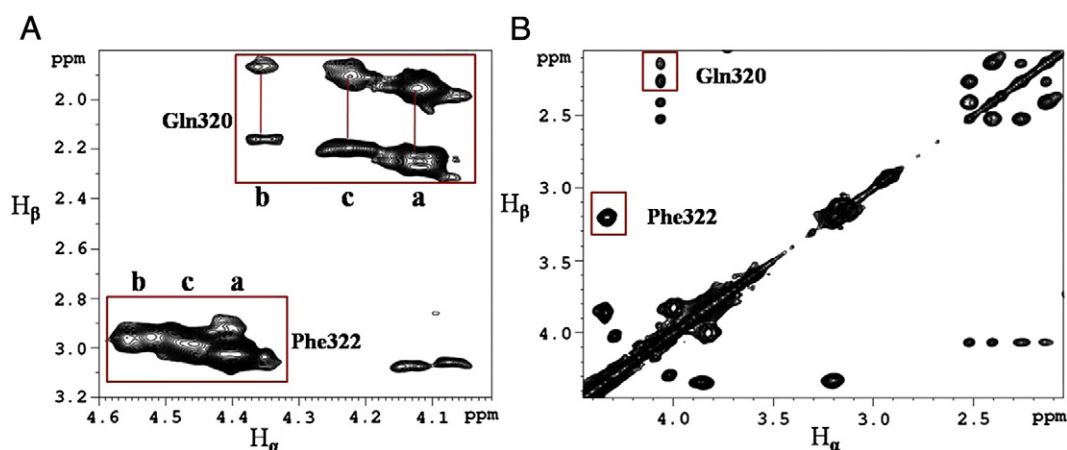
Fig. 1. A) H_α–H_β region from a 500 MHz TOCSY spectrum (44 ms mixing time) of 1 mM Shaw2 L45 in 10 mM sodium phosphate, pH* = 3.0 with 20% TFE at 293 K. The box marks the H_α–H_β cross peaks of Gln320 and Phe322. Labels indicate α-helical conformation, a; β-sheet, b and random coil, c. B) H_α–H_β region TOCSY spectrum (45 ms mixing time) of 1 mM Shaw2 L45 in 30 mM DPC, 10 mM sodium phosphate, pH* = 5.8 at 302 K. Gln320 correlations to δ and γ protons are also visible below the box.

Δ (d20), the spoil gradient (p19) and gradient length δ (p30). All gradients were applied as half sine shapes. Δ (d20) of 200 ms and p19 of 1.1 ms (−6.2 G/cm) were chosen for all 2D DOSY acquisitions, δ (p30) was set as 2.2 ms and 3.5 ms for peptide without and with micelles, respectively. The actual strength (g) of the half sine shaped gradients was varied from 0.735 to 34.9 G/cm. Typically, 256 scans and a data matrix of 8K × 16 were recorded. The spectra were processed using the Bruker AU program (dosy2d) and data were fitted to the equation below with XWINNMR T_1/T_2 software:

$$I = I_0 \cdot e^{-D(\gamma g \delta)^2 (\Delta - \delta/3)} \tag{5}$$

where I_0 is unattenuated signal intensity, D is the diffusion coefficient, γ is the gyromagnetic ratio of the observed nucleus, in this case $\gamma(^1H) = 4.258 * 10^3$ Hz/G.

3.3. Structure calculations

The 3D structure was calculated by utilizing DYANA (DYnamics Algorithm for NMR Applications) [42]. Cross peak volumes of a 75 ms NOESY were used as input for CALIBA to obtain distance restraints. This information together with 12 $^3J_{NH-H\alpha}$ constants extracted from 1D spectra were used for local conformational analysis and generation of final distance constraints (total 197) and angle constraints (total 60) in HABAS following established protocols [42]. The final structures were generated through 3000 steps stimulated annealing using a standard setup and visualized with the program Molmol [43] or Pymol.

4. Results/discussion

4.1. Shaw2 L45 structure in TFE studied by CD and NMR spectroscopy

To examine how readily Shaw2 L45 assumes an α-helix, TFE was used to probe the extent and location of helix formation. In the absence of TFE, L45 is only partially structured [28]. Upon increasing the TFE concentration the peptide gradually assumes an α-helical conformation. Noticeably, no isodichroic point could be observed, therefore the transition cannot be analyzed using a simple two-state model. The 44 ms TOCSY spectrum of Shaw2 L45 in the presence of 20% TFE (Fig. 1A) clearly reveals the coexistence of three different conformations. This is supported by the three distinct sets of TOCSY cross peaks between H_α and side chain H_β protons for both Gln320 and Phe322. For both residues, the most downfield shifted TOCSY pattern represents a β-strand conformation; the middle correlation is attributed to its random coil state and the most upfield indicates α-helical conformation.
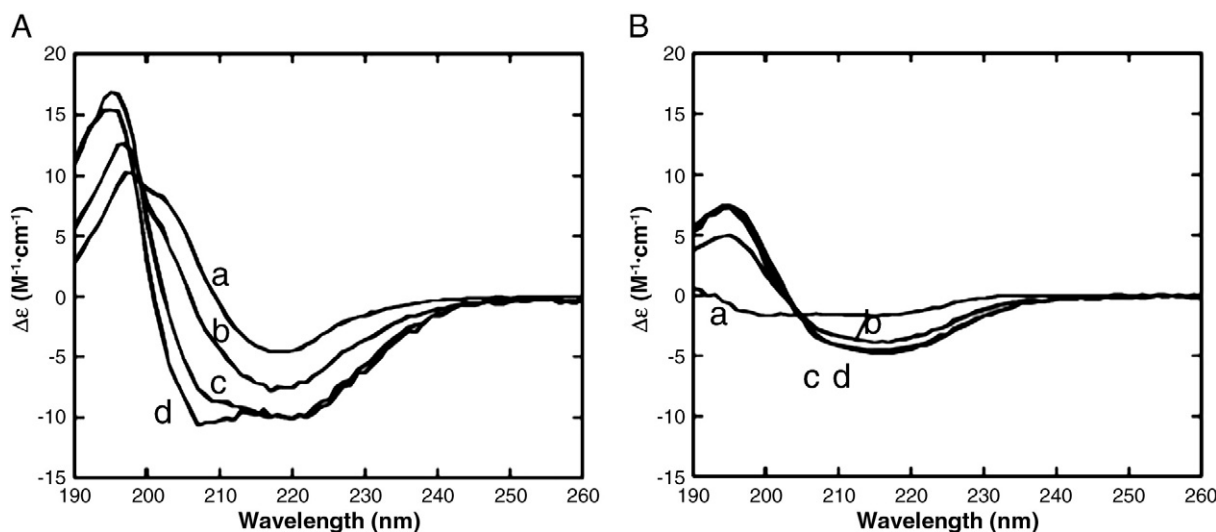

Fig. 2. CD spectra of A) L45 and B) S6c in the presence of increasing DPC concentrations (a: 1.5 mM, b: 3.0 mM, c: 20 mM and d: 30 mM DPC).
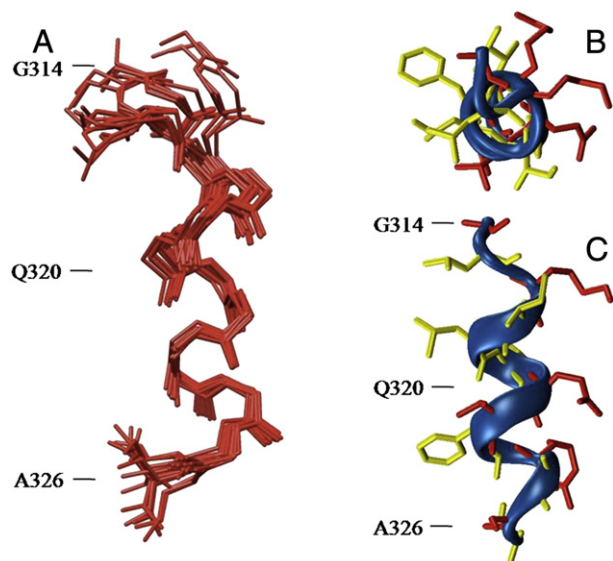
Fig. 3. Shaw2 L45 NMR structure in DPC micelles generated by DYANA. A total of 40 structures were generated. The mean backbone RMSD is 0.96 ± 0.33 Å, and 1.44 ± 0.27 Å for the mean heavy atom. The resulting structures were visualized with Pymol. A) 20 conformers with the lowest target function (from $3.13 \ast 10^{-2}$ to $9.07 \ast 10^{-2}$). B) Top view of the lowest energy conformer in cartoon mode. Hydrophobic residues are shown in yellow and polar side chains are in red. C) Side view.

The chemical shift index method (CSI) [44] provided a more detailed picture of the location and growth of the α-helix of Shaw2 L45 as a function of the TFE concentration (SI Table S1). In the absence of TFE, CSI indicates the presence of an α-helix from Gln320 to Ala326. As the TFE concentration increases the α-helix grows to encompass Ile319 and then Leu318 and finally fills in to the N terminus. This signifies the presence of a stable α-helix at the C-terminus that grows towards the N-terminus.

4.2. Structure of Shaw2 L45 in DPC micelles

CD spectra of the Shaw2 L45 in micelles (Fig. 2A) revealed α-helical characteristics. The α-helical content, as judged by the ellipticity at 208 nm, increases upon raising the DPC concentration and plateaus around 20 mM DPC. This is attributed to micelle packing [45]. The α-helical content of L45 at 20 and 30 mM of DPC is calculated to be 79.3% and 83.4%, respectively. In DMPC/DHPC bicelles (SI Fig. S1) L45 is also α-helical but at a lower content.

The NMR structure of the Shaw2 L45 in 30 mM DPC micelles was generated from 197 distance and 60 torsion angle restraints (SI Table S2). As expected a substantial number of medium-range connectivities, e.g. H_α proton of residue i to amide protons of residue $i + 3$ and/or $i + 4$, which is characteristic of an α-helical structure were observed while no long-range constraints are evident (SI Fig. S2). Calculations were then performed using the DYANA macro anneal and structures were visualized with Pymol. A regular α-helix is formed from residues Ile317 to Ser325 while the helix is less ordered at the C-terminus and is disrupted at the N-terminus (Fig. 3). This is either due to dynamics or a consequence of fewer constraints at that location. A Ramachandran plot confirmed that most of the phi and psi angles fall in the area of the α-helix favored region (SI Fig. S3). In contrast to the structure of L45 in 20% TFE (Fig. 1A), we did not observe any evidence suggesting the presence of more than one conformation of L45 in DPC micelles (Fig. 1B).

4.3. Solvent exposure and orientation of Shaw2 L45 in DPC micelles

The solvent accessibility of Shaw2 L45 in DPC micelles can be probed with paramagnetic reagents. These reagents effectively relax exposed NMR active nuclei, while nuclei that are buried in a micelle are protected. In this study the Gd-DTPA-BMA contrast agent was chosen because the large organic moiety that chelates Gd^{3+} attenuates the relaxation enhancement compared to a naked paramagnetic ion. In addition, this reagent was shown to not interact with either membranes or proteins [46–48]. Fig. 4A lists the ratio of T_1 values of L45 H_α protons obtained from inversion-recovery ^{13}C-^{1}H HSQC in the presence and absence of Gd-DTPA-BMA (SI Table S3). In the presence of the reagent, Gly314, Lys316, Ile317, Ile319, Gln320 and Arg323 show a large decrease in the T_1 value, indicative of solvent accessibility. In contrast, Leu315, Leu318, Phe322 and Ala326 were only marginally affected, suggesting that they are buried in the micelle.

The solvent accessibility can be further explored using the paramagnetic attenuation method presented previously [38,39]. In this analysis, residues with an A_i greater than 1.39 are classified as highly accessible, residues with $1.39 \geq A_i \geq 0.61$ have moderate accessibility and residues with <0.61 are considered protected. As expected the

A

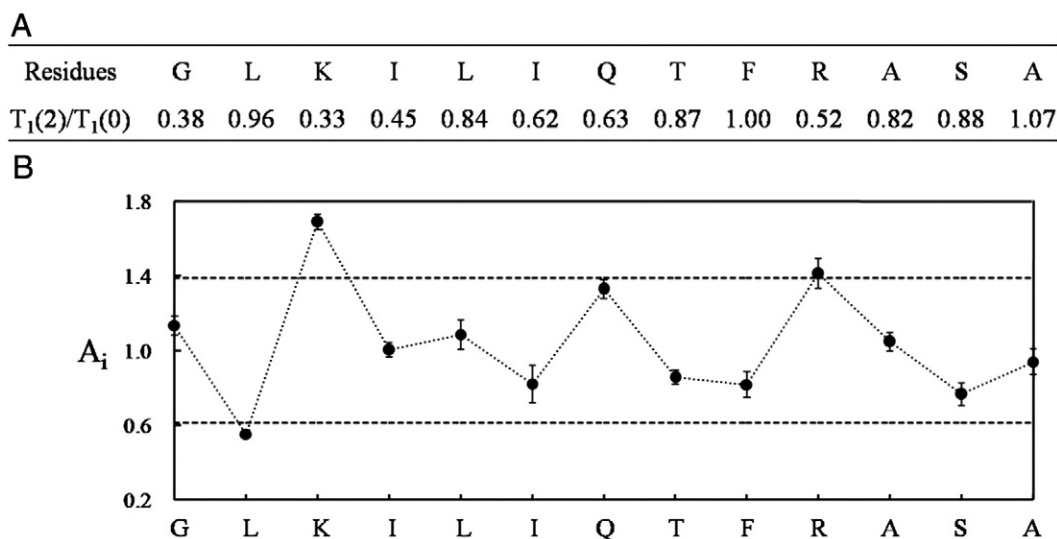| Residues	G	L	K	I	L	I	Q	T	F	R	A	S	A
$T_1(2)/T_1(0)$	0.38	0.96	0.33	0.45	0.84	0.62	0.63	0.87	1.00	0.52	0.82	0.88	1.07

Fig. 4. A) T_1 ratio of L45 H_α protons. $T_1(0)$ and $T_1(2)$ are T_1 of L45 H_α protons in the absence or presence of 2 mM of Gd-DTPA-BMA. B) Paramagnetic attenuation A_i of L45 H_α protons versus residue number.
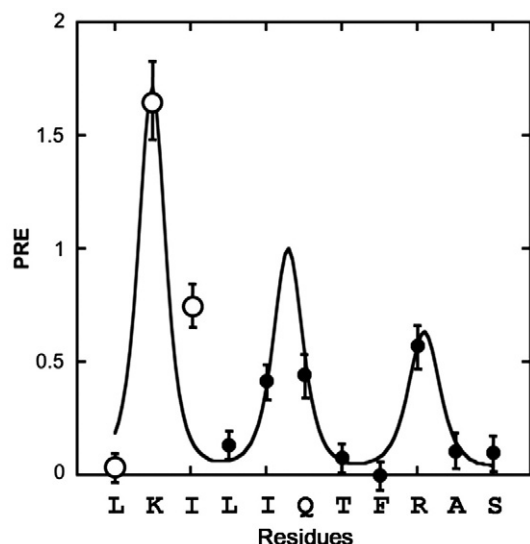
Fig. 5. PRE analysis of Shaw2 L45 in DPC micelles. Data for residue L318 to S325 were used for fitting Eq. 4. Errors were derived from the nonlinear least squares fit.

H_α of charged residues Lys316 and Arg323 are highly accessible while H_α of Leu315 is considered protected. All other residues with $1.39 \geq A_i \geq 0.61$ are intermediate (Fig. 4B). Qualitative T_1 values (data not shown) obtained from saturation-recovery NOESY experiments for H_γ protons also indicate that the side chains of Ile319 and Gln320 are solvent exposed while Thr321 is partially shielded.

To probe the orientation of an α-helical peptide in a micelle a previously described method was applied [40]. Briefly, paramagnetic relaxation enhancements (PREs) computed from the T_1's of each H_α in the presence and absence of the paramagnetic reagent were used to extract tilt angle (τ), immersion depth (A) and rotation (ρ) of the peptide in the micelle by fitting the PRE data to Eq. (4). The effects of immersion depth, rotation and tilt angle on the PRE are explored using a model α-helical system described in Supplementary material (SI Fig. S4). For the fitting of the PRE of L45 only Leu318 to Ser325 were considered because this approach requires a regular α-helical structure (Fig. 5). As shown in Fig. 6, the immersion depth A of the H_α proton of Leu318, the first residue in the calculation, was calculated to be 7.0 ± 1.5 Å and it points towards the center of the micelle with a rotation angle ρ of $206 \pm 4.0°$. The helix tilt angle, τ is $6.9 \pm 2.8°$. Considering the surface curvature of a DPC micelle with a diameter of ~40 Å [49], we can conclude that L45 is bound to the surface and nearly parallel to it as shown in Fig. 6. According to orientation and residue accessibility data, Leu315, Leu318, Phe322 and Ala326 are buried inside the micelle while the charged residues Lys316 and Arg323, and the polar residue Gln320 face towards the solution and Thr321 and Ser325 are at the interface.
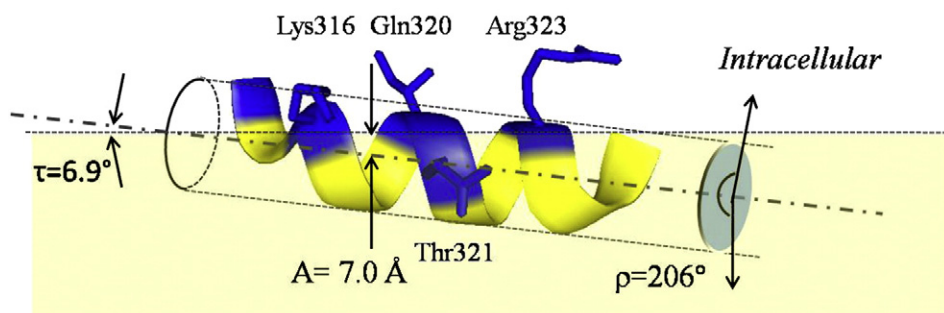
4.4. Structural features of S6c in TFE and micelles

Unlike L45, the CD spectra of S6c upon TFE titration display a two-state transition from random coil to α-helix (SI Fig. S5). It also requires more TFE (~80%) to obtain 50% α-helical conformation than is needed for L45, signifying a lower α-helical propensity of S6c. In both DPC micelles and DMPC/DHPC bicelles S6c adopts a partial α-helix (Fig. 2B and SI Fig. S1). Specifically, the helical content plateaus at just 39.4% at 20 mM DPC (Fig. 2B). The lower α-helicity is also manifest in the peptide dynamics in micelles. This is supported by the line width and the small chemical dispersion of the peptide resonances (SI Fig. S6). In addition, and in contrast to L45, no α-helical characteristics ($^3J_{NH-H\alpha}$, NOESY connectivity) were observed. Therefore we conclude that this peptide adopts a more disordered and dynamic structure.

4.5. Potential alkanol binding sites on Shaw2 L45 and S6c

Upon the addition of a small amount of 1-butanol (1–5 mM) to Shaw2 L45 in micelles we observed H_N chemical shift changes (~0.03 ppm) for Gln320, Thr321, Phe322 and Arg323 (Fig. 7). This appears to be specific for 1-butanol since methanol did not produce any chemical shift changes in the range tested (up to 10 mM, data not shown). A related observation is that the addition of 10% TFE (~1.4 M) to Shaw2 L45 in micelles produced an additional NOE contact between H_N of Gln320 and Thr321. This implies that Gln320 and Thr321 are sensing the presence of 1-butanol and TFE and may act as a site of interaction for such molecules. Similarly, C_α and H_α chemical shift changes induced by high TFE concentrations again map to Thr321. These results are in good agreement with a recent mutagenesis study of L45 where mutating Thr321 to alanine had a negative effect on the modulation of the channel by 1-butanol [30]. We note that the local chemical shift changes are quite small and are consistent with only minor local structural changes but would not support helix disruption or unwinding.

1-Butanol titration of S6c in DPC micelles also revealed a small chemical shift change (~0.02 ppm) of Thr423 and Gln424 amide protons in the presence of just 2 mM 1-butanol indicating that these residues may interact with 1-butanol while all the other amide protons were insensitive (SI Fig. S6).

4.6. Organization of L45, S6c and 1-butanol on micelles

Diffusion measurements using 2D DOSY can aid in exploring intermolecular interaction [50]. As shown in Table 1, the L45 showed a 58% decrease in the diffusion constant (15.6×10^{-11} to 6.6×10^{-11} m^2 s^{-1}) in the presence of micelles. Similarly, the diffusion constant of S6c is also greatly lowered in micelles. This further demonstrates that both L45 and S6c are micelle associated. Furthermore, the lower diffusion constant measured for L45 when S6c is added suggests that both the peptides can coexist on the

Fig. 6. Orientation of Shaw2 L45 in micelles. The micelle is represented by the light shaded region. *A*, immersion depth; ρ, rotation; τ, helix tilt angle. Blue indicates polar peptide residues while yellow signifies hydrophobic amino acids.
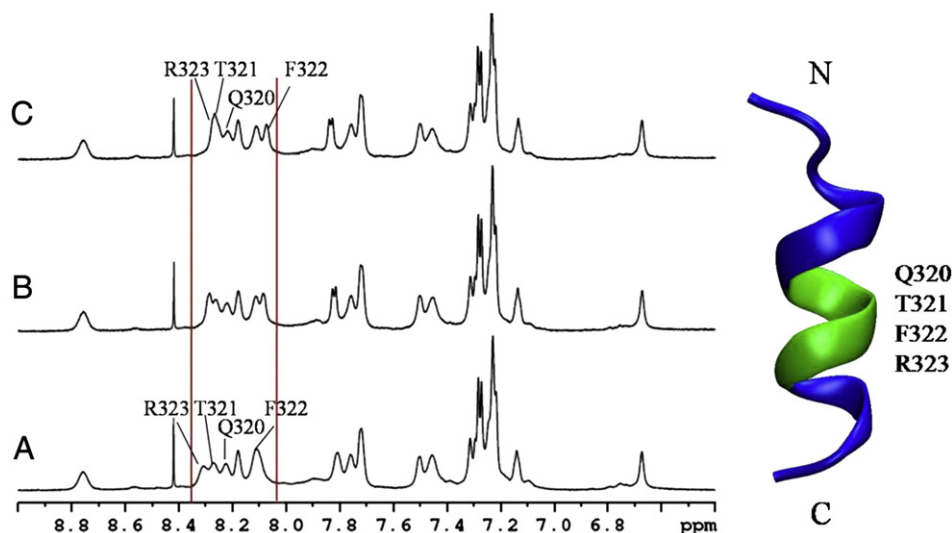
Fig. 7. Left panel: change of the 1D NMR H_N region of L45 in micelles upon 1-butanol titration at 303 K. A, L45 in micelles. B, L45 peptide in micelles with 1 mM 1-butanol. C, L45 peptide in micelles with 5 mM 1-butanol. Right panel: L45 NMR structure cartoon with mapped 1-butanol induced chemical shift changes (light green).

same micelle. The slightly lower diffusion constant of 1-butanol (65.1 to $57.3*10^{-11}$ m^2 s^{-1}) also indicates its association with the micelles part of the time. This property may facilitate the interaction of 1-butanol with peptide residues that are located at the interface or inside micelles. However, the interaction of 1-butanol with the L45–S6c peptide pair could not be observed in this system. We note that the peptides may distribute unevenly among the micelles, which may complicate an interpretation.

5. Conclusions

The response of Shaw2 Kv channels to 1-alkanols is dependent on the S4–S5 linker peptide, as the binding for 1-butanol is coupled to its α-helix propensity of the linker region [28]. Both CD and NMR experiments established that L45 adopts an α-helical conformation in DPC micelles.

The solvent accessibility and angular orientation of Shaw2 L45 on micelles was determined using paramagnetic perturbation methods. The results substantiate that the linker peptide resides on the membrane surface and lies essentially parallel to it. Surface accessibility experiments suggest that the hydrophobic residues (Leu315, Leu318, and Phe322) are located inside the micelle, while Lys316, Gln320, and Arg323 face towards the solution. The combination of the surface location of L45, the α-helical conformation and the orientation as well as the fact that it is important for channel function make it an attractive and accessible molecular target. The other important component

of the alkanol response, S6c, in contrast to L45, only forms a partial α-helix as observed by CD spectroscopy. Moreover NMR data reveals that the α-helix is not stable on the NMR time scale.

Diffusion constant measurements confirmed that L45, S6c and 1-butanol can associate with micelles, which encourages an interaction among the components. Chemical shift perturbations implicate residues Gln320, Thr321, Phe322 and Arg323 on L45 and Thr423 and Gln424 on S6c as potential 1-butanol binding candidates. This finding along with the fact that 1-butanol is capable of interacting with micelles suggests that membrane associated 1-butanol might perturb the interaction of S6c and L45. Canonical models of voltage-dependent gating can explain how this perturbation stabilizes the channel's closed state to produce inhibition [51]. In Shaker-related Kv channels, such as Shaw2, the activation gate prefers its closed conformation [52]. It is therefore necessary to apply force to open it. Upon depolarization of the membrane potential, the voltage sensors adopt their "up" conformation and pull on L45, which acts as the "handle" that actively opens the activation gate through its interaction with S6c. 1-Butanol and other inhaled anesthetics may dislodge this interaction and, consequently, the channel remains closed [25].

Although the mechanism of the gating and inhibition of Shaw2 Kv channel is complex and requires the participation of all four monomers that must be embedded in a cell membrane for function, our results shed light on the local structure and interaction of key components of the Shaw2 Kv channel, which governs the 1-alkanol sensitivity of the entire channel.

Table 1
Diffusion measurements of L45, S6c, micelles and 1-butanol at 293 K. Samples were prepared in 10 mM sodium phosphate, 99.96% D_2O (pH* $= 4.0$). The diffusion constant of HDO servers as an internal reference. Diffusion constants are given in [m^2 s^{-1}].

Sample	HDO (10^{-11})	1-Butanol (10^{-11})	L45 (10^{-11})	S6c (10^{-11})	DPC (10^{-11})
1-Butanol (4 mM)	156	65.1 ± 0.5			
DPC (30 mM)	154				7.8 ± 0.2
1-Butanol + DPC	154	57.5 ± 0.3			7.8 ± 0.13
L45 (~1 mM)	152		15.6 ± 0.6		
L45 + DPC	154		6.6 ± 0.1		7.5 ± 0.12
L45 + DPC + 1-butanol	156	56.8 ± 2	6.5 ± 0.15		7.6 ± 0.1
S6c (~0.6 mM)	158			15.6 ± 0.1	
S6c + DPC	158			7.6 ± 0.05	7.9 ± 0.25
L45 + S6c + DPC + 1-butanol	159	59.6 ± 0.2	6.2 ± 0.1	NA	7.7 ± 0.2

Acknowledgements

Appendix A. Supplementary

Supplementary data to this article can be found online at http://dx.doi.org/10.1016/j.bbamem.2012.09.025.

References

[1] G.A. Gutman, K.G. Chandy, S. Grissmer, M. Lazdunski, D. Mckinnon, L.A. Pardo, G.A. Robertson, B. Rudy, M.C. Sanguinetti, W. Stuhmer, X. Wang, International Union of Pharmacology. LIII. Nomenclature and molecular relationships of voltage-gated potassium channels, Pharmacol. Rev. 57 (2005) 473–508.

[2] F.M. Ashcroft, From molecule to malady, Nature 440 (2006) 440–447.

[3] C.-C. Shieh, M. Coghlan, J.P. Sullivan, M. Gopalakrishnan, Potassium channels: molecular defects, diseases, and therapeutic opportunities, Pharmacol. Rev. 52 (2000) 557–593.

[4] P.E. MacDonald, M.B. Wheeler, Voltage-dependent K^+ channels in pancreatic beta cells: role, regulation and potential as therapeutic targets, Diabetologia 46 (2003) 1046–1062.

[5] F. Bezanilla, The voltage sensor in voltage-dependent ion channels, Physiol. Rev. 80 (2000) 555–595.

[6] Y. Jiang, A. Lee, J. Chen, V. Ruta, M. Cadene, B.T. Chait, R. MacKinnon, X-ray structure of a voltage-dependent K^+ channel, Nature 423 (2003) 33–41.

[7] S.B. Long, E.B. Campbell, R. MacKinnon, Crystal structure of a mammalian voltage-dependent Shaker family K^+ channel, Science 309 (2005) 897–903.

[8] S.B. Long, X. Tao, E.B. Campbell, R. MacKinnon, Atomic structure of a voltage-dependent K^+ channel in a lipid membrane-like environment, Nature 450 (2007) 376–382.

[9] M.M. Pathak, V. Yarov-Yarovoy, G. Agarwal, B. Roux, P. Barth, Closing in on the resting state of the shaker K^+ channel, Neuron 56 (2007) 124–140.

[10] A.J. Labro, A.L. Raes, A. Grottesi, D.V. Hoorick, M.S.P. Sansom, D.J. Snyders, Kv channel gating requires a compatible S4–S5 linker and bottom part of S6, constrained by non-interacting residues, J. Gen. Physiol. 132 (2008) 667–680.

[11] M. Han, J.Z.H. Zhang, Molecular dynamic simulation of the Kv1.2 voltage-gated potassium channel in open and closed state conformations, J. Phys. Chem. B 112 (2008) 16966–16974.

[12] S.-Y. Lee, A. Banerjee, R. MacKinnon, Two separate interfaces between the voltage sensor and pore are required for the function of voltage-dependent K^+ channels, PLoS Biol. 7 (2009) 0676–0686.

[13] Z. Batulan, G.A. Haddad, R. Blunck, An intersubunit interaction between S4–S5 linker and S6 is responsible for the slow off-gating component in Shaker K^+ channels, J. Biol. Chem. 285 (2010) 14005–14019.

[14] A.J. Labro, I.R. Boulet, F.S. Choveau, E. Mayeur, T. Bruyns, G. Loussouarn, A.L. Raes, D.J. Snyders, The S4–S5 linker of KCNQ1 channels forms a structural scaffold with the S6 segment controlling gate closure, J. Biol. Chem. 286 (2011) 717–725.

[15] Z. Lu, A.M. Klem, Y. Ramu, Coupling between voltage sensors and activation gate in voltage-gated K^+ channels, J. Gen. Physiol. 120 (2002) 663–676.

[16] M.Ø. Jensen, V. Jogini, D.W. Borhani, A.E. Leffler, R.O. Dror, D.E. Shaw, Mechanism of voltage gating in potassium channels, Science 336 (2012) 229–233.

[17] M.L. Garcia, G.J. Kaczorowski, Potassium channels as targets for therapeutic intervention, Sci. STKE 2005 (2005) e46.

[18] R. MacKinnon, S.L. Cohen, A. Kuo, A. Lee, B.T. Chait, Structural conservation in prokaryotic and eukaryotic potassium channels, Science 280 (1998) 106–109.

[19] K.L. Choi, C. Mossman, J. Aubé, G. Yellen, The internal quaternary ammonium receptor site of shaker potassium channels, Neuron 10 (1993) 533–541.

[20] M. Covarrubias, A. Bhattacharji, T. Harris, B. Kaplan, M.W. German, Alcohol and anesthetic action at the gate of a voltage-dependent K^+ channel, in: Basic and Systemic Mechanisms of Anesthesia, International Congress Series, 1283, Elsevier, The Netherlands, 2005, pp. 55–60.

[21] G.C.L. Bett, R.L. Rasmusson, Modification of K^+ channel–drug interactions by ancillary subunits, J. Physiol. 586 (2008) 929–950.

[22] J.J.L. Hodge, J.C. Choi, C.J. O'Kane, L.C. Griffith, Shaw potassium channel genes in *Drosophila*, J. Neurobiol. 63 (2005) 235–254.

[23] M. Covarrubias, E. Rubin, Ethanol selectively blocks a noninactivating K^+ current expressed in *Xenopus* oocytes, Proc. Natl. Acad. Sci. U. S. A. 90 (1993) 6957–6960.

[24] T. Harris, M. Shahidullah, J.S. Ellingson, M. Covarrubias, General anesthetic action at an internal protein site involving the S4–S5 cytoplasmic loop of a neuronal K^+ channel, J. Biol. Chem. 275 (2000) 4928–4936.

[25] A. Bhattacharji, N. Klett, R.C.V. Go, M. Covarrubias, Inhalational anesthetics and n-alcohols share a site of action in the neuronal Shaw2 Kv channel, Br. J. Pharmacol. 159 (2010) 1475–1485.

[26] M. Covarrubias, T.B. Vyas, L. Escanar, A. Wei, Alcohols inhibit a cloned potassium channel at a discrete saturable site. Insight into the molecular basis of general anesthesia, J. Biol. Chem. 270 (1995) 19408–19416.

[27] M. Shahidullah, T. Harris, M.W. Germann, M. Covarrubias, Molecular features of an alcohol binding site in a neuronal potassium channel, Biochemistry 42 (2003) 11243–11252.

[28] A. Bhattacharji, B. Kaplan, T. Harris, X. Qu, M.W. German, M. Covarrubias, The concerted contribution of the S4–S5 linker and the S6 segment to the modulation of a K_v channel by 1-alkanols, Mol. Pharmacol. 70 (2006) 1542–1554.

[29] T. Harris, A.R. Graber, M. Covarrubias, Allosteric modulation of a neuronal Kv channel by 1-alkanols is linked to a key residue in the activation gate, Am. J. Physiol. Cell Physiol. 285 (2003) C788–C796.

[30] A.F. Barber, Q. Liang, C. Amaral, W. Treptow, M. Covarrubias, Molecular mapping of general anesthetic sites in a voltage-gated ion channel, Biophys. J. 101 (2011) 1613–1622.

[31] O. Ohlenschläger, H. Hojo, R. Ramachandran, M. Görlach, P.I. Haris, Three-dimensional structure of the S4–S5 segment of the shaker potassium channel, Biophys. J. 82 (2002) 2995–3002.

[32] S. Gayen, Q. Li, C. Kang, The solution structure of the S4–S5 linker of the hERG potassium channel, J. Pept. Sci. 18 (2011) 140–145.

[33] N. Sreerama, S.Y. Venyaminov, R.W. Woody, Estimation of protein secondary structure from circular dichroism spectra: inclusion of denatured proteins with native proteins in the analysis, Anal. Biochem. 287 (2000) 243–250.

[34] N. Sreerama, R.W. Woody, Estimation of protein secondary structure from circular dichroism spectra: comparison of CONTIN, SELCON, and CDSSTR methods with an expanded reference set, Anal. Biochem. 287 (2000) 252–260.

[35] P. Plateau, M. Gueron, Exchangeable proton NMR without base-line distortion, using new strong-pulse sequences, J. Am. Chem. Soc. 104 (1982) 7310–7311.

[36] T.D. Goddard, D.G. Kneller, SPARKY 3, University of California, San Francisco, 2008.

[37] K. Wüthrich, NMR of Proteins and Nucleic Acids, First ed. A Wiley-Interscience Publication, New York, 1986.

[38] H. Molinari, G. Esposito, L. Ragona, M. Pegna, N. Niccolai, R.M. Brunne, A.M. Lesk, L. Zetta, Probing protein structure by solvent perturbation of NMR spectra: the surface accessibility of bovine pancreatic trypsin inhibitor, Biophys. J. 73 (1997) 382–396.

[39] V. Venditti, A. Bernini, A.D. Simone, O. Spiga, F. Prischi, N. Niccolai, MD and NMR studies of α-bungarotoxin surface accessibility, Biochem. Biophys. Res. Commun. 356 (2007) 114–117.

[40] M. Respondek, T. Madl, C. Göbl, R. Golser, K. Zabgger, Mapping the orientation of helices in micelle-bound peptides by paramagnetic relaxation waves, J. Am. Chem. Soc. 129 (2007) 5228–5234.

[41] R. Kerssebaum, DOSY and diffusion by NMR, XWinNMR 3.1/3.5 Version 1.03, Bruker BioSpin GmbH, Rheinstetten, Germany, 2002.

[42] P. Güntert, C. Mumenthaler, K. Wüthrich, Torsion angle dynamics for NMR structure calculation with the new program DYANA, J. Mol. Biol. 273 (1997) 283–298.

[43] R. Koradi, M. Billeter, K. Wüthrich, MOLMOL: a program for display and analysis of macromolecular structures, J. Mol. Graph. 14 (1996) 51–55.

[44] D.S. Wishart, B.D. Sykes, F.M. Richards, The chemical shift index: a fast and simple method for the assignment of protein secondary structure through NMR spectroscopy, Biochemistry 31 (1992) 1647–1651.

[45] P.K. Mandal, J.W. Pettegrew, Alzheimer's disease: soluble oligomeric Aβ(1–40) peptide in membrane mimic environment from solution NMR and circular dichroism studies, Neurochem. Res. 29 (2004) 2267–2272.

[46] G. Pintacuda, G. Otting, Identification of protein surfaces by NMR measurements with a paramagnetic Gd(III) chelate, J. Am. Chem. Soc. 124 (2002) 372–373.

[47] S.K. Morcos, Nephrogenic systemic fibrosis following the administration of extracellular gadolinium based contrast agents: is the stability of the contrast agent molecule an important factor in the pathogenesis of this condition? Br. J. Radiol. 80 (2007) 73–76.

[48] K. Zangger, M. Respondek, C. Göbl, W. Hohlweg, K. Rasmussen, G. Grampp, T. Madl, Positioning of micelle-bound peptides by paramagnetic relaxation enhancements, J. Phys. Chem. B 113 (2009) 4400–4406.

[49] D. Clayton, I.M. Brereton, P.A. Kroon, R. Smith, NMR studies of the low-density lipoprotein receptor-binding peptide of apolipoprotein E bound to dodecylphosphocholine micelles, Protein Sci. 8 (1999) 1797–1805.

[50] L.H. Lucas, C.K. Larive, Measuring ligand–protein binding using NMR diffusion experiments, Concepts Magn. Reson. Part A 20A (2004) 24–41.

[51] V. Vardanyan, O. Pongs, Coupling of voltage-sensors to the channel pore: a comparative view, Front. Pharmacol. 3 (2012) 145–154.

[52] O. Yifrach, R. MacKinnon, Energetics of pore opening in a voltage-gated K^+ channel, Cell 111 (2002) 231–239.